Synthesis of Full Poincaré beams by means of uniaxial crystals

G Piquero[1], L Monroy[1], M Santarsiero[2], M Alonzo[3] and J C G de Sande[4]

[1] Departamento de Óptica, Universidad Complutense de Madrid, 28040 Madrid, Spain

[2] Dipartimento di Ingegneria, Universitá Roma Tre, Rome, Italy

[3] Dipartimento SBAI, Università Sapienza, Via A. Scarpa 16, 00161 Roma, Italy

[4] ETSIS de Telecomunicación, Universidad Politécnica de Madrid, Campus Sur, 28031 Madrid, Spain

E-mail: piquero@ucm.es

Abstract.

A simple optical system is proposed to generate full-Poincaré beams, i.e., beams presenting all possible states of (total) polarization across their transverse section. The method consists in focusing a uniformly polarized laser beam onto a uniaxial crystal having its optic axis parallel to the propagation axis of the impinging beam. A simple approximated model is used to obtain the analytical expression of the beam polarization at the output of the crystal. The output beam is then proved to be a full-Poincaré beam. By changing the polarization state of the input field, full-Poincaré beams are still obtained, but presenting different distributions of the polarization state across the beam section. Experimental results are reported, showing an excellent agreement with the theoretical predictions.

Keywords: Polarization, Full Poincaré beams, Singular optics

Submitted to: *J. Opt.*

1. Introduction

A subject that is presently receiving increasing attention is the generation of nonuniformily totally polarized (NUTP) light fields, whose use has also been proposed as a way to improve the performances of measurement techniques in different areas of Optics, such as microscopy, polarimetry, optical trapping, quantum information encoding, etc. [1–31].

A peculiar class of fields are the so called full-Poincaré beams (FPBs), which have been considered with particular attention in recent years [16, 17, 26, 30, 32–38]. The beams in which we are interested are NUPT beams that present all possible states of

totally polarized light across their transverse section. Different methods for generating them have been proposed and implemented, including the use of thermally stressed windows [32] and spatial light modulators (SLM) [35].

A simple method to obtain a FPB is proposed and demonstrated in this work. It is based on the propagation of a totally polarized incident laser beam along a uniaxial crystal having its optic axis parallel to the propagation direction of the incident beam, and input and output faces perpendicular to it. If the beam impinging onto the crystal is well approximated by a plane wave, of course, propagation does not change its polarization state, and the latter remains uniform across the output face of the crystal. But if the former presents a curvature, or if its transverse profile is not uniform, the propagation of ordinary and extraordinary waves within the crystal have to be considered, and the polarization state of the output beam in general depends on the position across the exit plane of the crystal, i.e., a NUTP beam is generated.

Propagation of Gaussian beams through uniaxial crystals can be studied in paraxial conditions, for example, by expanding the input beam in terms of plane waves and evaluating the contribution to the total exit field of all the produced plane waves (both ordinary and extraordinary) propagating through the crystal [22, 25, 39–44]. Such an approach has been used, for example, to study the generation of optical vortices in uniaxial crystals [41, 43], to study the conversion of spin to orbital angular momentum [7, 15, 42], or to obtain different engineered nonuniformly polarized beams at the output of the crystal [22, 25, 44].

Here, we use a much simpler approach, according to which the source of a spherical wave is located on the entrance face of the crystal, and the field across the exit face is evaluated through a geometrical-optics approach [4]. From the analysis of the corresponding Stokes parameters, we will show that the output beam belongs to the class of the FPBs. The used approximations are quite drastic but, as we shall see, they lead to very simple analytical expressions for the Jones vector of the output beam and, mostly, are in perfect agreement with the experimental results obtained when a laser beam is focused onto the entrance face of the crystal.

The paper is organized as follows: in Sec. 2 the theoretical model to calculate the polarization characteristics of the output beam is recalled, while Sec. 3 is devoted to prove that the output beam is a FPB for the particular case of a linearly polarized input beam. In Sec. 4 such result is extended to the case of a general input polarization. In Sec. 5 the approach is implemented and experimental results are presented, concerning the polarization distribution across the transverse section of the output beam. Finally, in Sec. 6 brief concluding remarks are given.

2. Theoretical model

Let us consider a uniformly and totally polarized beam, with a generically elliptical polarization state, propagating along the z-axis of a suitable reference frame. To simplify the following analysis, the beam is focused onto the input face of a uniaxial crystal of

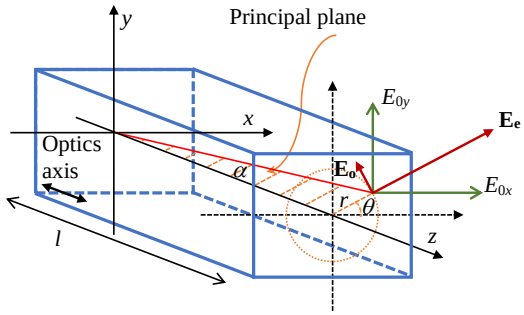

Figure 1. Crystal geometry. (r, θ) are the polar coordinates for a generic point at the output plane; α is the angle that the propagation direction from the input point to the generic point (r, θ) forms with the z axis; the optic axis is along z axis; the output field is decomposed in its Cartesian components (E_{0x}, E_{0y}) and in its ordinary and extraordinary fields, $\mathbf{E_o}$ and $\mathbf{E_e}$, respectively.

length l, having input and output faces perpendicular to z and optic axis parallel to it (see Fig. 1).

The focused spot of the beam will be considered as almost point-like. Let its electric field be written as

$$\mathbf{E_i} = \begin{pmatrix} E_{0x} \\ \\ E_{0y}\exp(\mathrm{i}\phi) \end{pmatrix}, \tag{1}$$

where E_{0x} and E_{0y} are the field components along x and y, respectively, and ϕ is the phase difference between them. The field at any point of polar coordinates (r, θ) of the output plane can be decomposed into a component of the electric field in the principal plane (the extraordinary wave) and a component of the electric field perpendicular to the principal plane (the ordinary wave) [45]. Neglecting refraction effects at the output boundary and losses at the input and output planes, the extraordinary and ordinary components of the electric field of the output beam are

$$\begin{aligned} \mathbf{E_e}(r,\theta) &= [E_{0x}\cos\theta + E_{0y}\sin\theta\exp(\mathrm{i}\phi)]\exp\left[\mathrm{i}kn(\alpha)d_e\right]\mathbf{u}_r\ , \\ \mathbf{E_o}(r,\theta) &= [-E_{0x}\sin\theta + E_{0y}\cos\theta\exp(\mathrm{i}\phi)]\exp\left[\mathrm{i}kn_o d_o\right]\mathbf{u}_\theta\ , \end{aligned} \tag{2}$$

where $\mathbf{u}_r$ and $\mathbf{u}_\theta$ are unitary vectors along the azimuthal and radial directions, respectively (see Fig. 1), k is the wavenumber in vacuum, n_o the ordinary refractive index, and $n(\alpha)$ is the refractive index for the extraordinary wave whose propagation direction forms the angle α with respect to the optic axis. This refractive index satisfies the following relation [45]:

$$\frac{1}{n^2(\alpha)} = \frac{\cos^2\alpha}{n_o^2} + \frac{\sin^2\alpha}{n_e^2}\,, \tag{3}$$

being n_e the extraordinary refractive index of the uniaxial crystal. For small values of α, the ordinary and the extraordinary waves practically propagate along the same

direction, so that they almost travel the same distance $d_e \simeq d_o \simeq d = \sqrt{l^2 + r^2}$.

The output field, expressed in terms of its x and y components, turns out to be

$$\mathbf{E}(r,\theta) = \begin{pmatrix} E_x(r,\theta) \\ E_y(r,\theta) \end{pmatrix} = \exp\left[-\mathrm{i}kd\,\frac{n(\alpha)+n_o}{2}\right] \tag{4}$$
$$\times \begin{pmatrix} E_{0x}\,\left[\cos^2\theta e^{\mathrm{i}\delta(r)/2} + \sin^2\theta e^{-\mathrm{i}\delta(r)/2}\right] + \mathrm{i}E_{0y}\,e^{i\,\phi}\sin 2\theta \sin\left[\delta(r)/2\right] \\ \\ \mathrm{i}E_{0x}\sin 2\theta\sin\left[\delta(r)/2\right] + E_{0y}e^{i\,\phi}\,\left[\cos^2\theta\; e^{-\mathrm{i}\delta(r)/2} + \sin^2\theta\; e^{\mathrm{i}\delta(r)/2}\right] \end{pmatrix},$$

where the phase difference $\delta(r)$ is [45]

$$\delta(r) \simeq k[n(\alpha) - n_o]d \simeq k(n_e - n_o)d\sin^2\alpha = k(n_e - n_o)\frac{r^2}{d}\,. \tag{5}$$

The Stokes parameters [45] at a typical point across the output plane can be derived from the electric field components through the following relations:

$$\mathbf{S} = \begin{pmatrix} S_0 \\ S_1 \\ S_2 \\ S_3 \end{pmatrix} = \begin{pmatrix} |E_x|^2 + |E_y|^2 \\ |E_x|^2 - |E_y|^2 \\ 2\,\mathrm{Re}\{E_x E_y^*\} \\ 2\,\mathrm{Im}\{E_x E_y^*\} \end{pmatrix}, \tag{6}$$

where $\mathrm{Re}\{\cdot\}$ and $\mathrm{Im}\{\cdot\}$ denote real and imaginary part, respectively, and for brevity the dependence on the spatial coordinates has been omitted. The first Stokes parameter (S_0) coincides with the total irradiance, while the three remaining parameters represent, respectively, the differences between the contents of linearly polarized light along the x and y axes, between the contents of linearly polarized light at 45^0 and -45^0, and between right-handed and left-handed circularly polarized contents of the beam [45].

The Stokes parameters can be obtained from intensity measurements, since [45]

$$\begin{aligned} S_0 &= I_0 + I_{\pi/2}, \\ S_1 &= I_0 - I_{\pi/2}, \\ S_2 &= I_{\pi/4} - I_{-\pi/4}, \\ S_3 &= I_{\lambda/4,\pi/4} - I_{\lambda/4,-\pi/4}, \end{aligned} \tag{7}$$

where I_β and $I_{\lambda/4,\beta}$ are the intensities measured after a linear polarizer and after a quarter-wave plate followed by a linear polarizer, respectively. The subscript β refers to the angle formed by the transmission axis of the polarizer with the x axis, while $\lambda/4$ denotes the presence of the quarter-wave plate, with its fast axis at 0.

If we restrict ourselves to the case of input light linearly polarized along the vertical direction (as the one that will be used in the experiment) with amplitude E_{0y}, the output beam takes the form

$$\mathbf{E}(r,\theta) = E_{0y}\,e^{-\mathrm{i}k\frac{n(\alpha)+n_o}{2}d} \begin{pmatrix} \mathrm{i}\,\sin 2\theta\sin\left[\delta(r)/2\right] \\ \\ \cos^2\theta e^{-\mathrm{i}\delta(r)/2} + \sin^2\theta e^{\mathrm{i}\delta(r)/2} \end{pmatrix}. \tag{8}$$

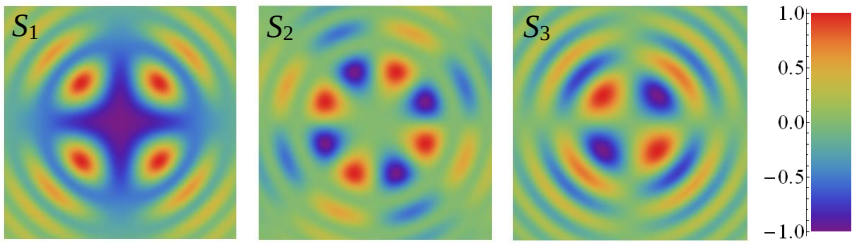

Figure 2. Theoretical values of the three Stokes parameters at the exit plane for an input beam linearly polarized along the y axis with 632.8 nm wavelength propagating in a 20 mm length calcite crystal.

The corresponding Stokes parameters are obtained by substituting the field given by Eq. (8) into Eq. (6), and turn out to be

$$\mathbf{S} = S_0 \begin{pmatrix} 1 \\ s_1 \\ s_2 \\ s_3 \end{pmatrix} = S_0 \begin{pmatrix} 1 \\ -[\cos^2 2\theta + \sin^2 2\theta \cos\delta(r)] \\ -\sin 2\theta \cos 2\theta \,[1 - \cos\delta(r)] \\ \sin 2\theta \, \sin\delta(r) \end{pmatrix}, \tag{9}$$

where the elements of the normalized Stokes vector, namely, $\mathbf{s} = \mathbf{S}/S_0$, have been introduced. It can be easily checked that the normalized Stokes parameters satisfy the following condition at any point across the section of the beam:

$$s_1^2 + s_2^2 + s_3^2 = 1\,, \tag{10}$$

meaning that the field is totally polarized at any point of the beam transverse section, as was expected.

As an example, the normalized Stokes parameters calculated from Eq. (9) at the output of a 20 mm long calcite crystal ($n_o = 1.6557$, $n_e = 1.4849$), with a 632.8 nm wavelength, are shown in Fig. 2. The chosen values of the parameters correspond to the ones used in the experiment.

3. Is the output beam a FPB?

As stated above, a FPB is a NUTP beam that contains all possible states of polarization across its transverse section [32]. This means that for any conceivable polarization state, represented by a point on the surface of the Poincaré sphere, it must be possible to find at least one point in the cross section of the beam that presents such state. This will be done for the case of the beam at the output of a uniaxial crystal under the geometry represented in Fig. 1.

Note that, since only totally polarized states are involved, the normalized Stokes parameters satisfy Eq. (10), so that only two of them are independent. If we choose s_1 and s_2 as the independent parameters, their values are confined within the equatorial circular section of the Poincaré sphere. The modulus of s_3 is fixed by Eq. (10), but its sign determines the handedness of the polarization state.

We will show that for any possible choice of s_1 and s_2 within the equatorial circle and for any choice of the sign of s_3, at least one point (r, θ) can be found where the field polarization is given by that set of Stokes parameters.

Let us start by writing s_1 in the following form [see Eq. (9)]:

$$s_1 = -1 + \sin^2 2\theta \, [1 - \cos \delta(r)] \, , \tag{11}$$

so that

$$1 - \cos \delta(r) = \frac{1 + s_1}{\sin^2 2\theta} \, . \tag{12}$$

Introducing the latter relation into the expression of s_2 yields

$$s_2 = - \, (1 + s_1) \, \frac{\cos 2\theta}{\sin 2\theta} \, , \tag{13}$$

and then

$$\tan 2\theta = -\frac{1 + s_1}{s_2} \, . \tag{14}$$

This means that four real values of θ, namely,

$$\theta = -\frac{1}{2} \arctan \left(\frac{1 + s_1}{s_2} \right) + j \, \frac{\pi}{2} \, , \qquad (j = 0, 1, 2, 3) \tag{15}$$

are compatible with a given choice of s_1 and s_2. However, two of such values correspond to a positive s_3 and the remaining two to a negative s_3. This can be argued from the expression of s_3 in Eq. (9), according to which, for any fixed value of r the sign of $\sin 2\theta$ fixes the sign of s_3. Therefore, changing θ to $\theta + \pi/2$ changes s_3 to $-s_3$. This fact can be checked from the graphs in Fig. 2.

Let us now take again the expression of s_3 in Eq. (9) into consideration and write it in the form

$$\sin 2\theta = \frac{s_3}{\sin \delta(r)} \, . \tag{16}$$

Once substituted into Eq. (12), it gives

$$1 - \cos \delta(r) = \frac{1 + s_1}{s_3^2} \left[1 - \cos^2 \delta(r) \right] = \frac{1 + s_1}{s_3^2} \left[1 - \cos \delta(r) \right] \left[1 + \cos \delta(r) \right] \, , \tag{17}$$

and then

$$\cos \delta(r) = \frac{s_3^2}{1 + s_1} - 1 = \frac{s_3^2 - 1 - s_1}{1 + s_1} = \frac{-s_1^2 - s_2^2 - s_1}{1 + s_1} \, , \tag{18}$$

where condition in Eq. (10) has been used.

Equation (18) allows us to find the value of δ that corresponds to a given choice of s_1 and s_2. From this value, the pertinent radial distance r is obtained on inverting Eq. (5). It should be noted that δ is proportional to r^2 [see Eq. (5)], with the proportionality factor depending on the wavelength and the used material and geometry. In any case, all possible values of $\cos \delta(r)$ are obtained for $\delta(r)$ varying between 0 and π, and are reached by taking r within a circle of radius

$$r_{\mathrm{M}} = \sqrt{\frac{\lambda d}{2|n_e - n_o|}} . \tag{19}$$

For a calcite crystal with the same length and using the same wavelength than that in Fig. 2, this radius is $r_{\rm M} \simeq 0.19$ mm.

What is still to be done is to show that Eq. (18) leads to a real value of δ for any choice of s_1 and s_2, that is, that the rhs expression in Eq. (18) is always bounded between -1 and 1:

$$-1 \leq \frac{-s_1^2 - s_2^2 - s_1}{1 + s_1} \leq 1\,. \tag{20}$$

The denominator of the central part is clearly non-negative (because $s_1 \geq -1$), so that Eq. (20) can be written as

$$-1 - s_1 \leq -s_1 - s_1^2 - s_2^2 \leq 1 + s_1\,. \tag{21}$$

The lhs inequality corresponds to

$$0 \leq 1 - s_1^2 - s_2^2 = s_3^2\,, \tag{22}$$

and is always satisfied, while the rhs inequality corresponds to

$$0 \leq 1 + 2s_1 + s_1^2 + s_2^2 = (1 + s_1)^2 + s_2^2\,, \tag{23}$$

which is certainly true as well.

We can conclude that for any arbitrary point on the surface of the Poincaré sphere at least two points exist across the transverse profile of the output beam, whose polar coordinates can be evaluated from Eqs. (15), (18), and (5), where the polarization state is the one defined by that point on the Poincaré sphere. Therefore, the beam given by Eq. (8) is a full-Poincaré beam.

This fact can be observed in Fig. 3, where ellipses of polarization are drawn for the field at different points across the transverse section of the output beam. Red ellipses denote right-handed polarization states while blue ellipses represent left-handed states. The presented results agree with those obtained in [44] using a different approach. It can be noticed that points at symmetric positions with respect to the beam center present the same polarization state. The solid semicircle in Fig. 3 has radius r_M and defines a region where all possible polarization states can be found.

It should be stressed that all the polarization states can also be found in the quarter circle of radius $\sqrt{2}\, r_M$, identified by a dashed line in Fig. 3. In such a case the angle θ spans the interval $(0, \pi/2)$ but the phase δ goes from zero to 2π.

To show that all possible polarization states are present in the semicircle shown in Fig. 3, it can be useful to represent such states on the Poincaré sphere. In Fig. 4(a), r varies in the interval $(0, r_M)$ for fixed values of the polar angle θ in the interval $(0, \pi)$. On changing r, the point representing the polarization state moves across the sphere surface forming a figure-8 contour around the equator with one lobe in each hemisphere (for right- and left-handed polarizations, respectively). This kind of contours are the same as those obtained for a fixed linear polarizer followed by a rotating linear retarder [46]. Figure-8 contours, but with a different shape and lobes along the orthogonal direction, are also obtained on varying θ for fixed values of r within the same intervals (Fig. 4(b)).

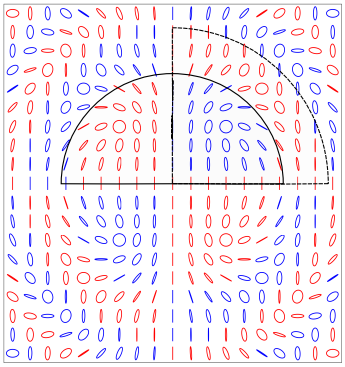

Figure 3. Polarization pattern of the beam at the output of a uniaxial crystal for an input beam linearly polarized along y. Same parameters than those for Fig. 2 have been used.

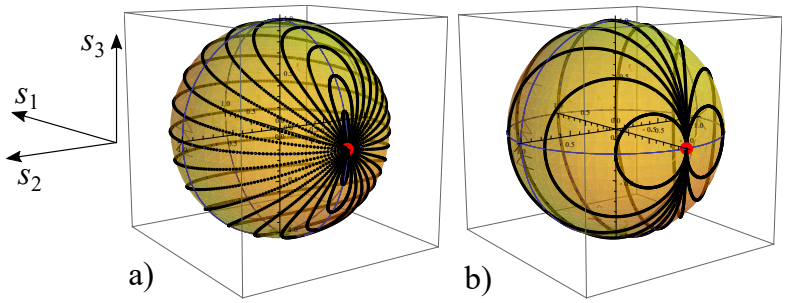

Figure 4. Poincaré sphere showing the states of polarization of the output beam for a linearly polarized input beam when different sets of points are selected inside a circle of radius r_M of the beam cross section: a) varying θ for 20 equally spaced r^2 values and b) varying r for 20 equally spaced θ angles. The red point at $(-1, 0, 0)$ represents the polarization state of the input beam.

4. Input beam with arbitrary state of polarization

For simplicity (and direct comparison with the experimental results), in the previous Section we chose the input state of polarization as linear, along the y direction. It is quite obvious, due to the axial symmetry of the problem, that analogous results would be obtained on taking the input field as linearly polarized along any direction in the transverse plane. But it can be easily shown that the output field is a FPB regardless of the polarization state of the input beam.

Starting from Eq. (4), the following expression of the Jones vector of the output field is derived for an arbitrary input field $\mathbf{E_i}$:

$$\mathbf{E}(r,\theta) = \exp\left[-\mathrm{i}kd\,\frac{n(\alpha)+n_o}{2}\right]\,\widehat{J}_C(r,\theta)\,\mathbf{E_i}\;. \tag{24}$$

Therefore, besides an unessential overall phase term, the effect of the uniaxial crystal is

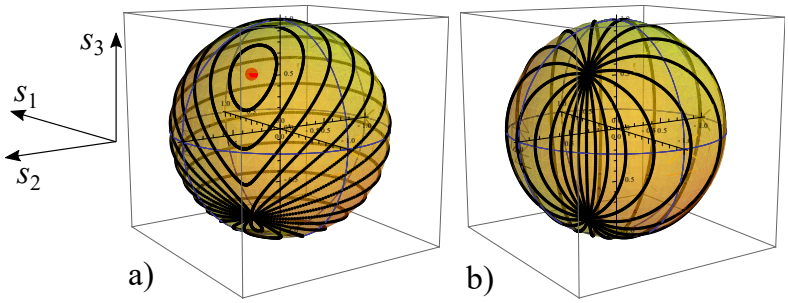

Figure 5. Poincaré sphere showing the states of polarization of the output beam for an input beam with a state of polarization given by $(s_1, s_2, s_3) = \left(-1, \sqrt{3/2}, \sqrt{3/2}\right)/2$, the red point, when different sets of points are selected inside a circle of radius r_M of the beam cross section: a) varying θ for 20 equally spaced r^2 values and b) varying r for 20 equally spaced θ angles.

represented by a Jones matrix, namely,

$$\widehat{J}_C(r,\theta) = \begin{pmatrix} \cos^2\theta e^{\mathrm{i}\delta(r)/2} + \sin^2\theta e^{-\mathrm{i}\delta(r)/2} & \mathrm{i}\sin 2\theta \sin\left[\delta(r)/2\right] \\ \mathrm{i}\sin 2\theta \sin\left[\delta(r)/2\right] & \cos^2\theta\, e^{-\mathrm{i}\delta(r)/2} + \sin^2\theta\, e^{\mathrm{i}\delta(r)/2} \end{pmatrix}, \quad (25)$$

depending on the position across the exit plane. It can be noted that the such Jones matrix corresponds to that of a phase wave plate, having retardance $\delta(r)$ and fast axis rotated by θ with respect to the x axis [47]. Therefore, in a semicircular region with radius r_M of the output beam cross section all possible values of the plate orientation and of its retardance can be found.

The effect on an arbitrary polarization state of a linear retarder, having retardance δ and fast axis rotated by θ, can be viewed on the Poincaré sphere as a rotation by the amount δ around an axis contained in the s_1, s_2 plane, forming the angle 2θ with respect to the s_1 axis [48]. Since, starting from any point of the Poincaré sphere, any other point on the sphere can be reached by means of such a transformation by suitably choosing retardance and orientation of the plate, then all possible polarization states will be present across the exit face of the crystal, regardless of the polarization state of the input beam.

This, in particular, gives account of the curves shown in Fig. 4, pertinent to the case of a linearly polarized input beam. On changing the polarization of the input beam, the polarization pattern across the section of the output beam changes [44], but the latter remains a FPB. This is graphically shown in Fig. 5, where results analogous to those in Fig. 4 are reported, but for an elliptically polarized input beam. Figure 6 shows the polarization patterns at the output plane for two different polarizations of the input beam: a) right circular polarization and b) elliptical polarization, the same as in Fig. 5.

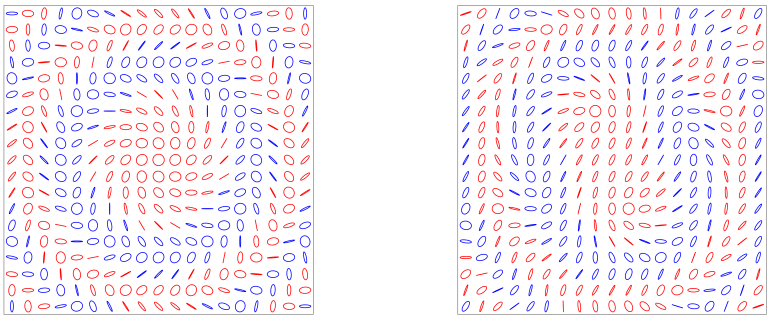

a) *b)*

Figure 6. Polarization patterns at the output of the crystal when the input beam is a) right circularly polarized or b) elliptically polarized with normalized Stokes parameters $(s_1, s_2, s_3) = \left(-1, \sqrt{3/2}, \sqrt{3/2}\right)/2$.

5. Experimental results

Here we present an experimental setup aimed at synthesizing a FPB using the technique described in the previous Sections. The beam is then produced and analyzed by measuring the local state of polarization across its transverse section at the exit face of the crystal.

Figure 7 shows the used experimental setup. A He-Ne laser ($\lambda = 632.8$ nm), stabilized in intensity and frequency, is linearly polarized along the y direction by means of the linear polarizer P_1. The microscope objective MO (5X) focuses the beam at the input face of a calcite crystal with its optic axis oriented along the z axis. The length of the crystal is $l = 20$ mm. The output beam is imaged onto a CCD camera (Pulnix TM-765) by means of the lens L.

In order to obtain the Stokes parameters of the output beam, four images are captured for different orientations of the transmission axis of the polarizer P_2 (0, $\pm\pi/4$ and $\pi/2$ with respect to the x direction). Two additional images are recorded when a quarter-wave phase plate ($\lambda/4$, in Fig. 7) is inserted when the polarizer is oriented at $\pm\pi/4$. By using the recorded images, the state of polarization at each point across the transverse section of the output beam is obtained from Eq. (7).

The experimentally measured (normalized) Stokes parameters across the transverse section of the beam at the output of the calcite crystal are shown in Fig. 8. They can be directly compared to the theoretical ones presented in Fig. 2. In order to get a better comparison, the state of polarization at each point of the transverse section of the beam has been calculated and represented by means of its corresponding ellipse of polarization. Figure 9 shows the experimentally measured polarization pattern across the beam section for output field in the same region than that of Fig.3. Again, red ellipses denote right-handed polarization states while blue ellipses represent left-handed states. An excellent agreement between experimental and theoretical values can be

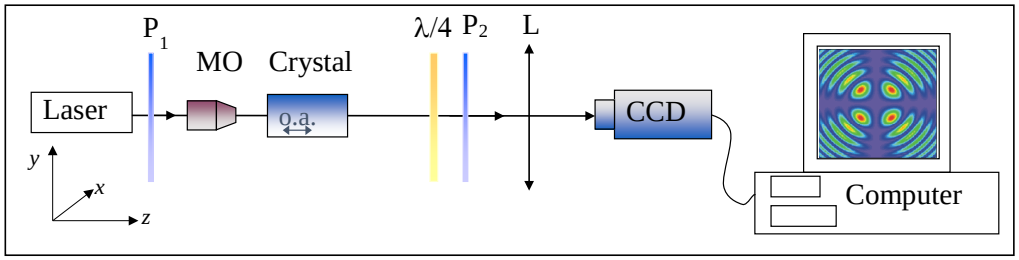

Figure 7. Experimental set up. MO: microscope objetive; $\lambda/4$: quarter-wave phase plate: P: linear polarizer; L: lens. The electric field of the laser beam is directed along y. The image on the computer represents a typical irradiance pattern recorded with the polarizer oriented along the x axis.

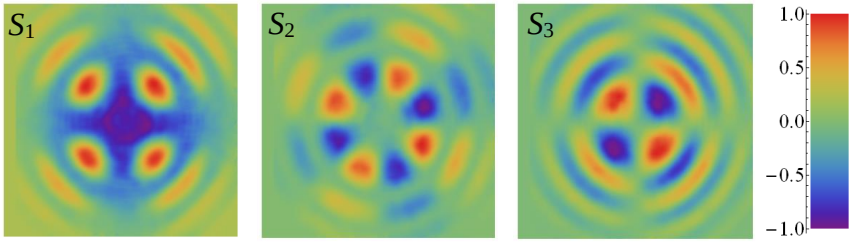

Figure 8. Experimental Stokes parameters at the output plane of a 20 mm length calcite crystal when a He-Ne laser beam linearly polarized along y is focused at the entrance face.

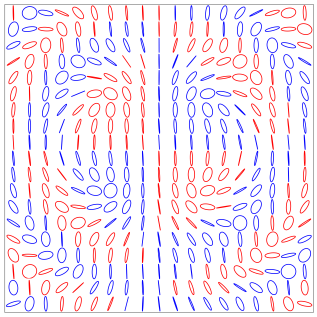

Figure 9. Experimental polarization pattern at the output of the calcite crystal for input linearly polarized beam along the y axis.

observed.

As a final remark, we stress that the good agreement between experimental and theoretical Stokes parameters represents an *a posteriori* confirmation that the used theoretical approach, with the considered approximations, can provide a simple and effective model for studying the generation of nonuninformly polarized beams at the output of a uniaxial crystal.

6. Conclusions

In this paper a simple technique has been proposed to obtain a FPB. It consists in focusing a totally and uniformly polarized light beam onto the entrance face of a uniaxial crystal, whose optic axis is oriented along the mean propagation direction of the beam. At the output of the crystal a beam with nonuniform polarization is obtained. The local state of polarization of the output beam is evaluated through a simplified model based on geometrical optics, and the result is that every possible state of total polarization is present across the transverse section of the output beam.

The proposed technique has been implemented by focusing a He-Ne laser beam onto a calcite crystal, and the polarization pattern at the exit face of the crystal has been measured, showing an excellent agreement between theoretical and and experimental data.

The significance of the results reported in the present paper is twofold. On one hand, they confirm that a simplified model based on the propagation of ordinary and extraordinary rays can be effectively employed to study beam propagation in anisotropic crystals in some cases of practical interest. On the other hand, they provide an extremely simple and cheap practical tool to produce FPBs in a lab. The latter beams may find application, for example, in polarimetry, where beams presenting several different polarization states across their transverse section can be used to reduce the number of measurements required to characterize homogeneous sample [49–51].

Acknowledgements

This work has been partially supported by Spanish Ministerio de Economía y Competitividad under project FIS2016-75147.

References

[1] Movilla J, Piquero G, Martínez-Herrero R and Mejías P 1998 *Optics Communications* **149** 230 – 234 ISSN 0030-4018 URL http://www.sciencedirect.com/science/article/pii/S0030401898000182

[2] Freund I 2001 *Optics Communications* **199** 47 – 63 ISSN 0030-4018 URL http://www.sciencedirect.com/science/article/pii/S0030401801015334

[3] Gori F 2001 *J. Opt. Soc. Am. A* **18** 1612–1617 URL http://josaa.osa.org/abstract.cfm?URI=josaa-18-7-1612

[4] Piquero G and Vargas-Balbuena J 2004 *European Journal of Physics* **25** 793 URL http://stacks.iop.org/0143-0807/25/i=6/a=011

[5] Korotkova O and Wolf E 2005 *Optics Communications* **246** 35 – 43 ISSN 0030-4018 URL http://www.sciencedirect.com/science/article/pii/S0030401804011058

[6] Niziev V G, Chang R S and Nesterov A V 2006 *Appl. Opt.* **45** 8393–8399 URL http://ao.osa.org/abstract.cfm?URI=ao-45-33-8393

[7] Marrucci L, Manzo C and Paparo D 2006 *Phys. Rev. Lett.* **96**(16) 163905 URL https://link.aps.org/doi/10.1103/PhysRevLett.96.163905

[8] Maurer C, Jesacher A, Frhapter S, Bernet S and Ritsch-Marte M 2007 *New Journal of Physics* **9** 78 URL http://stacks.iop.org/1367-2630/9/i=3/a=078

[9] Martínez-Herrero R and Mejías P M 2008 *Opt. Express* **16** 9021–9033 URL http://www.opticsexpress.org/abstract.cfm?URI=oe-16-12-9021
[10] Wang T and Pu J 2008 *Optics Communications* **281** 3617 – 3622 ISSN 0030-4018 URL http://www.sciencedirect.com/science/article/pii/S0030401808003052
[11] Zhan Q 2009 *Adv. Opt. Photon.* **1** 1–57 URL http://aop.osa.org/abstract.cfm?URI=aop-1-1-1
[12] Ramírez-Sánchez V, Piquero G and Santarsiero M 2009 *Journal of Optics A: Pure and Applied Optics* **11** 085708 URL http://stacks.iop.org/1464-4258/11/i=8/a=085708
[13] Ding C, Pan L and Lü B 2010 *Applied Physics B* **99** 307–315 ISSN 1432-0649 URL http://dx.doi.org/10.1007/s00340-009-3818-z
[14] Ramírez-Sánchez V, Piquero G and Santarsiero M 2010 *Optics Communications* **283** 4484 – 4489 ISSN 0030-4018 electromagnetic Coherence and Polarization URL http://www.sciencedirect.com/science/article/pii/S0030401810004220
[15] Marrucci L, Karimi E, Slussarenko S, Piccirillo B, Santamato E, Nagali E and Sciarrino F 2011 *Journal of Optics* **13** 064001 URL http://stacks.iop.org/2040-8986/13/i=6/a=064001
[16] Milione G, Sztul H I, Nolan D A and Alfano R R 2011 *Phys. Rev. Lett.* **107**(5) 053601 URL https://link.aps.org/doi/10.1103/PhysRevLett.107.053601
[17] Milione G, Evans S, Nolan D A and Alfano R R 2012 *Phys. Rev. Lett.* **108**(19) 190401 URL https://link.aps.org/doi/10.1103/PhysRevLett.108.190401
[18] de Sande J C G, Santarsiero M, Piquero G and Gori F 2012 *Opt. Express* **20** 27348–27360 URL http://www.opticsexpress.org/abstract.cfm?URI=oe-20-25-27348
[19] de Sande J C G, Piquero G and Teijeiro C 2012 *J. Opt. Soc. Am. A* **29** 278–284 URL http://josaa.osa.org/abstract.cfm?URI=josaa-29-3-278
[20] Vyas S, Kozawa Y and Sato S 2013 *Opt. Express* **21** 8972–8986 URL http://www.opticsexpress.org/abstract.cfm?URI=oe-21-7-8972
[21] Santarsiero M, de Sande J C G, Piquero G and Gori F 2013 *Journal of Optics* **15** 055701 URL http://stacks.iop.org/2040-8986/15/i=5/a=055701
[22] Shvedov V G, Hnatovsky C, Shostka N and Krolikowski W 2013 *J. Opt. Soc. Am. B* **30** 1–6 URL http://josab.osa.org/abstract.cfm?URI=josab-30-1-1
[23] de Sande J C G, Piquero G, Santarsiero M and Gori F 2014 *Journal of Optics* **16** 035708 URL http://stacks.iop.org/2040-8986/16/i=3/a=035708
[24] Zheng X, Lizana A, Peinado A, Ramírez C, Martínez J L, Márquez A, Moreno I and Campos J 2015 *J. Lightwave Technol.* **33** 2047–2055 URL http://jlt.osa.org/abstract.cfm?URI=jlt-33-10-2047
[25] Turpin A, Loiko Y V, Peinado A, Lizana A, Kalkandjiev T K, Campos J and Mompart J 2015 *Opt. Express* **23** 5704–5715 URL http://www.opticsexpress.org/abstract.cfm?URI=oe-23-5-5704
[26] Zhu W, Shvedov V, She W and Krolikowski W 2015 *Opt. Express* **23** 34029–34041 URL http://www.opticsexpress.org/abstract.cfm?URI=oe-23-26-34029
[27] McLaren M, Konrad T and Forbes A 2015 *Phys. Rev. A* **92**(2) 023833 URL https://link.aps.org/doi/10.1103/PhysRevA.92.023833
[28] Ndagano B, Sroor H, McLaren M, Rosales-Guzmán C and Forbes A 2016 *Opt. Lett.* **41** 3407–3410 URL http://ol.osa.org/abstract.cfm?URI=ol-41-15-3407
[29] Davis J A, Moreno I, Badham K, Sánchez-López M M and Cottrell D M 2016 *Opt. Lett.* **41** 2270–2273 URL http://ol.osa.org/abstract.cfm?URI=ol-41-10-2270
[30] Naidoo D, Roux F S, Dudley A, Litvin I, Piccirillo B, Marrucci L and Forbes A 2016 *Nature Photonics* **10** 327–332 URL http://dx.doi.org/10.1038/nphoton.2016.37
[31] Rubinsztein-Dunlop H, Forbes A, Berry M V, Dennis M R, Andrews D L, Mansuripur M, Denz C, Alpmann C, Banzer P, Bauer T, Karimi E, Marrucci L, Padgett M, Ritsch-Marte M, Litchinitser N M, Bigelow N P, Rosales-Guzmn C, Belmonte A, Torres J P, Neely T W, Baker M, Gordon R, Stilgoe A B, Romero J, White A G, Fickler R, Willner A E, Xie G, McMorran B and Weiner A M 2017 *Journal of Optics* **19** 013001 URL http://stacks.iop.org/2040-8986/19/i=1/a=013001

[32] Beckley A M, Brown T G and Alonso M A 2010 *Opt. Express* **18** 10777–10785 URL http://www.opticsexpress.org/abstract.cfm?URI=oe-18-10-10777
[33] Cardano F, Karimi E, Marrucci L, de Lisio C and Santamato E 2013 *Opt. Express* **21** 8815–8820 URL http://www.opticsexpress.org/abstract.cfm?URI=oe-21-7-8815
[34] Han W, Cheng W and Zhan Q 2011 *Opt. Lett.* **36** 1605–1607 URL http://ol.osa.org/abstract.cfm?URI=ol-36-9-1605
[35] Galvez E J, Khadka S, Schubert W H and Nomoto S 2012 *Appl. Opt.* **51** 2925–2934 URL http://ao.osa.org/abstract.cfm?URI=ao-51-15-2925
[36] Chen S, Zhou X, Liu Y, Ling X, Luo H and Wen S 2014 *Opt. Lett.* **39** 5274–5276 URL http://ol.osa.org/abstract.cfm?URI=ol-39-18-5274
[37] Wei C, Wu D, Liang C, Wang F and Cai Y 2015 *Opt. Express* **23** 24331–24341 URL http://www.opticsexpress.org/abstract.cfm?URI=oe-23-19-24331
[38] Colas D, Dominici L, Donati S, Pervishko A A, Liew T C, Shelykh I A, Ballarini D, de Giorgi M, Bramati A, Gigli G, del Valle E, Laussy F P, Kavolin A V and Sanvito D 2015 *Light: Science & Applications* **4** URL http://dx.doi.org/10.1038/lsa.2015.123
[39] Ciattoni A, Cincotti G and Palma C 2001 *Optics Communications* **195** 55 – 61 ISSN 0030-4018 URL http://www.sciencedirect.com/science/article/pii/S0030401801013359
[40] Cincotti G, Ciattoni A and Palma C 2001 *IEEE Journal of Quantum Electronics* **37** 1517–1524 ISSN 0018-9197
[41] Ciattoni A, Cincotti G and Palma C 2003 *J. Opt. Soc. Am. A* **20** 163–171 URL http://josaa.osa.org/abstract.cfm?URI=josaa-20-1-163
[42] Brasselet E, Izdebskaya Y, Shvedov V, Desyatnikov A S, Krolikowski W and Kivshar Y S 2009 *Opt. Lett.* **34** 1021–1023 URL http://ol.osa.org/abstract.cfm?URI=ol-34-7-1021
[43] Volyar A, Shvedov V, Fadeyeva T, Desyatnikov A S, Neshev D N, Krolikowski W and Kivshar Y S 2006 *Opt. Express* **14** 3724–3729 URL http://www.opticsexpress.org/abstract.cfm?URI=oe-14-9-3724
[44] Fadeyeva T A, Shvedov V G, Izdebskaya Y V, Volyar A V, Brasselet E, Neshev D N, Desyatnikov A S, Krolikowski W and Kivshar Y S 2010 *Opt. Express* **18** 10848–10863 URL http://www.opticsexpress.org/abstract.cfm?URI=oe-18-10-10848
[45] Born M and Wolf E 1980 *Principles of Optics* sixth (corrected) ed (Cambridge University Press) ISBN 0521639212
[46] Azzam R M A 2000 *J. Opt. Soc. Am. A* **17** 2105–2107 URL http://josaa.osa.org/abstract.cfm?URI=josaa-17-11-2105
[47] Goldstein D H 2003 *Polarized Light* second (revised and expanded) ed (Marcel Dekker, Inc.) ISBN 082474053X
[48] Sit A, Giner L, Karimi E and Lundeen J S 2017 *Journal of Optics* **19** 094003 URL http://stacks.iop.org/2040-8986/19/i=9/a=094003
[49] de Sande J C G, Santarsiero M and Piquero G 2017 *Optics and Lasers in Engineering* **91** 97 – 105 ISSN 0143-8166 URL http://www.sciencedirect.com/science/article/pii/S0143816616304171
[50] de Sande J C G, Piquero G and Santarsiero M 2018 *Optics Communications* **410** 961 – 965 ISSN 0030-4018 URL http://www.sciencedirect.com/science/article/pii/S003040181730888X
[51] Tripathi S and Toussaint K C 2009 *Opt. Express* **17** 21396–21407 URL http://www.opticsexpress.org/abstract.cfm?URI=oe-17-24-21396